Int J Earth Sci (Geol Rundsch) (2011) 100:1875–1893
DOI 10.1007/s00531-010-0627-x

SHORT NOTE

Whiting-related sediment export along the Middle Miocene carbonate ramp of Great Bahama Bank

Mélanie Turpin · Laurent Emmanuel · John J. G. Reijmer · Maurice Renard

Received: 28 May 2010 / Accepted: 20 November 2010 / Published online: 4 January 2011

Abstract Modern aragonite needles are present all along the modern leeward margin of Great Bahama Bank (ODP Leg 166), while Middle Miocene sediments contain needles only in more distal areas (Sites 1006 and 1007). In contrast to the rimmed, flat-topped platform topography during the Plio-Pleistocene, the Miocene Great Bahama Bank morphology is a carbonate ramp profile. This might imply a different location and precipitation type for Miocene aragonite needles. In this study, aragonite needles in Miocene sediments were isolated using a granulometric separation method. Furthermore, the isolation of the various carbonate components enables the identification of primary versus diagenetic components. The Miocene aragonite needles are concentrated in the finest granulometric sediment fractions (<12 μm). The fraction-specific geochemical analyses ($\delta^{13}C$, $\delta^{18}O$ and Sr elemental abundance) represent useful tools to assess the possible sources of the aragonite mud. The geochemical variation of the fractions, rich in pristine aragonite needles, and the characteristics of the needle morphology point to whiting phenomena as the main sediment source and algal fragmentation as a minor component. Both components indicate shallow-water environments as the main sediment source area. Ramp-top-related fine-grained particles now present at distal sites were likely exported as suspended material similar to present-day transport mechanisms. The scarcity of needles at proximal sites is probably linked to hydrodynamic processes but dissolution and recrystallization processes cannot be excluded. The granulometric separation approach applied here enables a better characterization of the finest carbonate particles representing an important step towards the discrimination between primary and diagenetic fine-grained components.

Keywords Aragonite needles · Whiting · Export process · Granulometric separation · Stable isotopes · Bahamas

M. Turpin · L. Emmanuel · M. Renard
Laboratoire Biominéralisations et Environnements sédimentaires, UPMC Paris 6, ISTep-UMR 7193, 4 Place Jussieu, 75252 Paris Cedex 05, France

J. J. G. Reijmer
Faculty of Earth and Life Sciences (FALW), Department of Sedimentology and Marine Geology, VU University Amsterdam, De Boelelaan 1085, 1081 HV Amsterdam, The Netherlands

Present Address:
M. Turpin (✉)
Institute for Geology, Mineralogy and Geophysics, Sedimentary and Isotope Geology, Ruhr-University Bochum, 44780 Bochum, Germany
e-mail: melanie.turpin@rub.de

Introduction

In the present-day tropical to subtropical carbonate factory, aragonite needles are an important component of micritic sediments (Lowenstam and Epstein 1957; Mathews 1966; Stockman et al. 1967). For example, aragonite needles represent up to 85–90% of the fine sediments on the Bahama banks (Milliman 1974; Heath and Mullins 1984; Reijmer et al. 2009). Their origin has been extensively discussed with authors supporting a biogenic origin and others favouring inorganic precipitation. Neumann and Land (1975; Bay of the Abaco–Bahamas) and Stockman et al. (1967; South Florida) estimate that a large part of the aragonite is produced by disintegration of codiacean algal thalli (in particular *Halimeda*) that frequently occur in protected shallow-water areas. Conversely, Cloud (1962a)

and Bathurst (1975) estimated that algal aragonite represents less than 5% of the total carbonate production on Great Bahama Bank (GBB) and concluded that most of the aragonite results from inorganic precipitation from seawater. Scanning electron microscope (SEM) studies (Loreau 1982; Macintyre and Reid 1992, 1995) documented that only 25–40% of the codiacean algae crystals possess a needle shape, whereas the majority of these features consist of equant nanograins. This suggests that the predominant volume of the modern GBB aragonite mud results from direct precipitation.

More recently, several authors (Macintyre and Reid 1992; Robbins and Blackwelder 1992; Robbins et al. 1997; Yates and Robbins 1999; Shinn et al. 2000, 2004; Thompson 2000) have proposed an alternative explanation for the formation of these needles in modern shallow-water sediments of GBB, namely whitings. Whitings are milky patches of suspended material with dimensions varying between several hundred metres to several kilometres in diameter and are mainly known from tropical and subtropical settings (Bahamas: Cloud 1962a, b; Broecker and Takahashi 1966; Shinn et al. 1989—Persian Gulf: Wells and Illing 1964; De Groot 1965—Dead Sea: Neev and Emery 1967—Belize: Mazzulo et al. 1995; Purdy and Gischler 2003). Whitings have also been described from lake environments (Great Lakes: Strong and Eadie 1978—Otisco Lake: Effler and Johnson 1987—Fayetteville Green Lake: Thompson and Ferris 1990; Thompson et al. 1997; Thompson 2000—Croatian marine lake: Sondi and Juračič 2010). In the case of precipitation from seawater, a bio-induced production is generally favoured, triggered by picoplankton (Thompson and Ferris 1990; Robbins and Blackwelder 1992; Robbins et al. 1996; Thompson et al. 1997; Yates and Robbins 1999; Thompson 2000; Sondi and Juračič 2010), as opposed to a spontaneous inorganic physicochemical precipitation from seawater. Several authors also propose that whitings are mainly composed of re-suspended sediment (Broecker and Takahashi 1966; Morse et al. 1984; Broecker et al. 2000).

Studies of the Middle Miocene periplatform sediments from the leeward flank of GBB (ODP Leg 166, Fig. 1; Eberli et al. 1997) have shown the occurrence of aragonite needles in the pelagic facies of the distal sites (basin: Site 1006 and toe-of-slope: Site 1007; Turpin et al. 2008). In contrast, these needles are absent in the proximal sites (upper and middle slope: Sites 1005 and 1003; Turpin 2006; Turpin et al. 2008). While modern Bahamian aragonite needles are present in all leeward settings and are linked to their production site on the bank top, the exclusive occurrence of Middle Miocene aragonite needles in the distal part of the sedimentary apron off the Great Bahama Bank questions their origin. The morphology of the Middle Miocene platform was ramp-like, the precipitation process and the spatial occurrence of aragonite could thus have differed from the Plio-Pleistocene rimmed, flat-topped platform type. The questions that need to be addressed in this respect are (1) whether Miocene aragonite needles represent similar precipitation phenomena to that of the modern needles and (2) what is the significance of the Miocene Bahamian ramp morphology relative to the present-day rimmed-margin in terms of aragonite needle formation and distribution.

Previous studies used the geochemical signature of carbonate ooze particles in order to evaluate the origin of these precipitates (Immenhauser et al. 2002; Minoletti et al. 2005; Turpin 2006; Beltran et al. 2009; Preto et al. 2009).

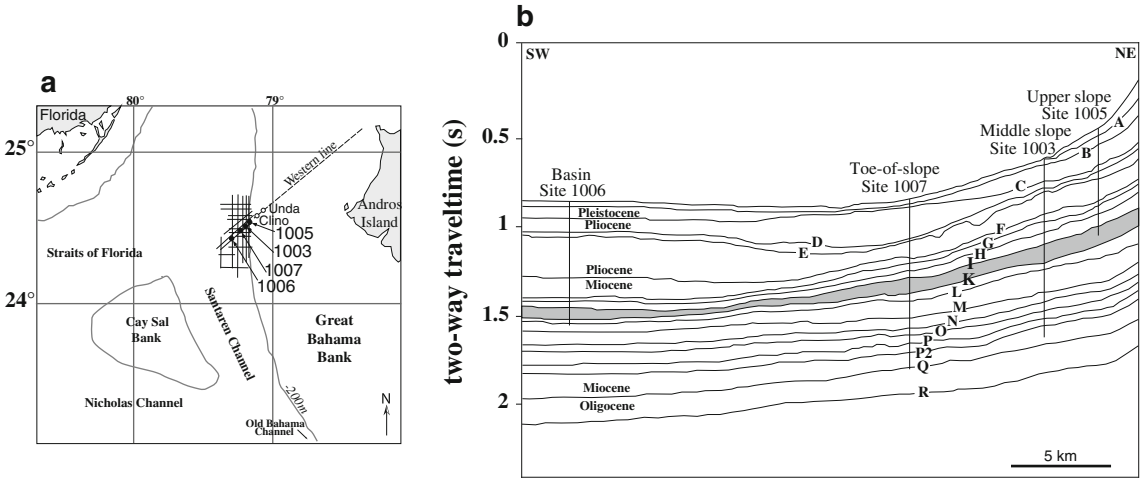

Fig. 1 **a** Location map of ODP Leg 166 and BDP drill sites on the leeward flank of Great Bahama Bank (after Eberli et al. 2002). **b** Interpreted seismic cross-section showing carbonate sequences across the leeward margin of Great Bahama Bank. Sequence boundaries are labelled A-I and K-R, and location of Bahamas Transect sites drilled during ODP Leg 166 is shown. The studied sequence K is shown in grey (modified from Eberli et al. 1997)

The evaluation of bulk carbonates isotope values, however, is complicated by the fact that analyses of mud-sized carbonates provide a geochemical average of a wide range of carbonate materials representing different depositional environments. In order to circumvent this problem, granulometric separation of specific carbonate particles is a useful way forward. The approach used here relies on granulometric separation of Middle Miocene bulk sediments with the aim to isolate carbonate particles of various size fractions with specific focus on aragonite needles. A detailed analysis of the <12 μm fractions, which concentrate aragonite needles, allows for the quantification and the characterization of the aragonite needles and also provides sample material for geochemical analysis.

The objectives of this study are threefold: (1) to determine the environment of production (basin vs. bank) of the Middle Miocene aragonite needles; (2) to characterize the process of needle precipitation (fragmentation of biological structures, whiting phenomenon); and (3) to compare their origin in the Middle Miocene ramp context to those occurring within the Plio-Pleistocene rimmed carbonate platform setting. The significance of this research is that it allows for a much more specific focus on individual components of carbonate oozes. This has important implications for palaeo-environmental interpretations due to the separation of primary characteristics from secondary (diagenetic) artefacts.

Geological setting and material

Seven holes (Sites 1003–1009) were drilled along the leeward flank of Great Bahama Bank during ODP Leg 166 (Eberli et al. 1997; Fig. 1). Five of these sites (Sites 1003–1007) form a platform/basin transect in the Straits of Florida through prograding carbonate sequences (ranging from the Upper Oligocene to the Holocene). Eberli et al. (1997) distinguished 17 seismic sequences within the Neogene succession ('A' to 'R'; Fig. 1), each with a duration of 1–1.5 Myr. The duration of these seismic sequences suggests that they record Neogene third-order sea-level changes (Anselmetti et al. 2000). Thirty five samples were collected (Table 1) through Middle Miocene seismic sequence K (≈11.7–10.7 Myr) in Holes 1005C (upper slope), 1003C (middle slope), 1007C (toe-of-slope) and in Hole 1006A, the most distal site situated in the Santaren Channel (approximately 30 km from the western, leeward, platform edge of the GBB). The sampled sequence corresponds to calcareous nannofossil zones NN7 and NN8, equivalent to planktonic foraminifer zones N13 to N16 (Eberli et al. 1997). Sediments of the basinal Site 1006 consist of soft carbonate oozes, whereas sediments of the toe-of-slope Site 1007 correspond to an alternation of densely and weakly cemented intervals (mudstones and some wackestones). At Sites 1006 and 1007, the average amount of <63 μm fraction is equal to 92 and 81% and the <12 μm fraction represents 71 and 61%, respectively. Sediments of slope Sites 1005 and 1003 consist of densely cemented mudstones and wackestones. At these Sites 1005 and 1003, the mean amount of <63 μm fraction is equal to 67 and 69% and the <12 μm fraction represents 41 and 46%, respectively. For a detailed description of composition per fraction, please refer to Turpin et al. (2008). At Site 1007, numerous authors (Betzler et al. 1999, 2000; Frank and Bernet 2000; Isern and Anselmetti 2001; Reuning et al. 2002) related the cyclic sedimentation pattern to sea-level fluctuations. The unlithified sediments, dominated by pelagic material and slightly affected by diagenesis, were related to sea-level lowstands. In contrast, lithified sedimentary rocks, characterized by an enhanced supply of neritic material from the bank and affected by a rapid cementation due to their metastable mineralogies,

Table 1 Number, depth, and degree of lithification of the Great Bahama Bank samples studied

Site 1005			Site 1003			Site 1007			Site 1006		
Sample number	Depth (mbsf)	Sample induration	Sample number	Depth (mbsf)	Sample induration	Sample number	Depth (mbsf)	Sample induration	Sample number	Depth (mbsf)	Sample induration
18R01	544.76	Lithified	08R02	523.15	Lithified	21R02	495.72	Unlithified	62X05	569.30	Unlithified
20R03	565.96	Lithified	09R02	532.46	Lithified	21R06	500.68	Lithified	63X03	575.90	Unlithified
21R02	573.68	Lithified	10R01	541.50	Lithified	23R01	513.75	Unlithified	63X05	578.90	Unlithified
22R01	581.77	Lithified	12R01	559.75	Lithified	23R07	520.99	Unlithified	65X01	592.25	Unlithified
23R01	591.12	Lithified	13R01	569.77	Lithified	24R04	527.57	Lithified	66X01	601.77	Unlithified
24R02	601.14	Lithified	14R01	579.81	Lithified	24R06	530.56	Lithified	67X05	617.50	Unlithified
25R03	611.52	Lithified	15R02	590.36	Lithified	26R01	542.55	Lithified	68X03	624.10	Unlithified
26R02	619.73	Lithified	17R02	609.77	Lithified	26R07	549.57	Lithified			
28R01	636.37	Lithified	18R02	619.71	Lithified	27R01	552.10	Lithified			
						27R03	554.50	Unlithified			

were related to sea-level highstands. These lithological variations might reflect sea-level fluctuations with a periodicity of 23,000–19,000 years, which can be correlated to the precessional cycle (Eberli et al. 1997; Betzler et al. 1999; Reuning et al. 2002). This type of sedimentation was also observed for the Plio-Pleistocene period but differences exist in the sediment nature (texture, composition, colour) compared to the Miocene deposits. These differences have been attributed to the early Pliocene change in platform morphology from a distally steepened ramp to a steep-sided platform (Beach and Ginsburg 1980; Eberli and Ginsburg 1989; Reijmer et al. 1992; Betzler et al. 1999; Eberli 2000; Reijmer et al. 2002). The Miocene carbonate ramp was characterized by a gentle, gradual topography from the top to the slope with a maximal angle of 4° (Eberli et al. 1997; Betzler et al. 1999). The morphology of the platform margin thus plays an important role in the composition of periplatform sediments.

Methodology

Granulometric separation

The granulometric separation method used in this study was first described in Minoletti et al. (2005) and was originally developed for the analysis of pelagic sediments. Here, the granulometric separation is applied to periplatform sediments. The samples (10 g of sediment) are first disaggregated and brought into suspension in an ultrasonic bath. The duration of this procedure depends on the degree of lithification of the sediments. For lithified intervals (Holes 1005C, 1003C and 1007C), samples are subjected to a preliminary crushing phase prior to disaggregation.

The sample preparation is accomplished in two steps. The first phase consists of wet sieving through 63- and 20-μm sieves to remove larger particles such as microfossils. In the second phase, the resulting suspension is size-separated in a sequence of filtration steps. Depending on the composition of the samples, four filtration steps were applied in an ultrasonic bath through etched-polycarbonate membrane filters with a micropore diameter of 12, 8, 5, and 3 μm. Finally, the finest particles (<3 μm) are concentrated by centrifuging. At the end of this procedure, seven granulometric fractions are isolated from each sample. This study focuses on the 12–8 μm, 8–5 μm, 5–3 μm, and <3 μm fractions of thirty-five samples and thus discusses the analysis of 140 separated fractions.

Smear slides were prepared for each separated grain-size fraction. The surface area of 200 randomly selected carbonate particles can be measured under a light microscope using a cross-grid to quantify the composition of each fraction. Even under a high magnification, the component characterization and quantification of the <3 μm fractions is rather difficult because of the small size of the particles. In this case, the evaluation of the abundance and the surface of the components were quantified using Scanning Electron Microscopy (SEM). Each <3 μm fraction was prepared on an etched-polycarbonate membrane filter with a micropore diameter of 0.4 μm. Based on the surface area quantification, the $CaCO_3$ content and the weight of different fractions, the proportion of each component in the bulk carbonate fraction is calculated.

X-ray diffractometry

X-ray diffraction was used to determine the mineralogy of the sediments and particularly the 12–8 μm, 8–5 μm, 5–3 μm, and <3 μm grain-size fractions. To obtain reproducible diffraction results, the grain size of the individual sediment fractions was reduced by grinding in an agate mortar. The analysis was carried out on a Siemens D501 X-ray diffractometer containing a copper anode. Runs are made from 3°2θ to 75°2θ with a counting step of 0.05°2θ/s and a 1 s counting time per step. Semi-quantitative mineralogical analysis was made with the MacDiff 4.2.5 software (Petschik 1991) using the digitized diffractograms. These show that two or three carbonate minerals coexist in the sediments: low-magnesium calcite (LMC), aragonite and dolomite. The peak-area method is deployed to quantify the aragonite content (Milliman 1974). The aragonite/calcite peak-area ratios were converted into relative weight percentages using an in-house calibration curve. Weight percentages of LMC and dolomite were calculated directly by their peak-area ratios. Diffraction peak-areas are corrected by the I/Icor coefficient resulting from PDF (Powder Data File) provided by the ICDD (International Center Diffraction Data). Mineralogy of particles is determined by the analysis of enriched fractions in each component and also using an EDS microprobe. Carbonate content of bulk sediments and separated fractions are analysed by XRD. Multiple analyses showed absolute deviations less than 4%.

Strontium content

Separated fractions were analysed for their Sr content using flame atomic absorption spectrometry (AAS, Hitachi Z8100). Samples are leached in 500 μl of pure nitric acid at 80°C. After filtering and rinsing, the resulting solution (with a concentration of 1%v/v. of nitric acid) is considered to represent the calcite and aragonite phase. The remaining solids are clays and oxides. Calibration of the AAS was achieved by means of a Sr standard solution. The standard and sample solutions are matrix corrected for Ca. Analytical precision on contents expressed in ppm is generally less than 5%.

Carbon and oxygen isotope analysis

Carbon ($\delta^{13}C$) and oxygen ($\delta^{18}O$) isotope compositions from various separated fractions were analysed (3–5 mg of sediment). The extraction of CO_2 was performed by reaction with anhydrous orthophosphoric acid at 50°C in an off-line system. Isotopic analyses are performed in a mass spectrometer Finnigan Delta E at UPMC (France). Carbon and oxygen isotope values are expressed in per mil relative to the V-PDB standard. Average standard deviation based on analyses of a reference standard is estimated to ±0.1‰ for oxygen and ±0.05‰ for carbon.

Any reader is welcome to directly contact the first author for accessing to the entire dataset.

Results

Mineralogy and particle type

Description and interpretation

The mean carbonate content of the bulk sediments is 77, 82, 85, and 79% at Sites 1006, 1007, 1003, and 1005, respectively. The remaining phase of the sediments consists of clays and oxides. Low-magnesium calcite dominates the carbonate phase with mean values of 87 and 79% for unlithified sediments at Sites 1006 and 1007, and 90, 98, and 96%, respectively, for lithified sediments at Sites 1007, 1003, and 1005 (Table 2). Aragonite is the second most abundant mineral at Sites 1006 and 1007 making up on average 12 and 19% of the carbonate fraction of unlithified sediments at both sites and 8% of lithified sediments at Site 1007. The aragonite does not occur at proximal Sites 1003 and 1005. Dolomite comprises only 1% of the carbonate fraction at Site 1006, 2% at Sites 1007 and 1003, and 4% at Site 1005.

In the carbonate phase, five types of carbonate particles have been identified (Table 2), which can be subdivided in two groups (1) low-Mg calcite biogenic particles and (2) particles lacking evidence for a biogenic origin. Below, the different types of low-Mg calcite biogenic particles (foraminifera, calcareous nannofossils, neritic debris) are detailed:

Foraminifera (in the >63 μm and 63–20 μm fractions), whole tests or fragments, are mainly of planktonic origin (*Orbulina*, *Globigerinoides, Globorotalia, Globoquadrina*, and *Globigerina*). Benthic foraminifera (*Lenticulina*, *Cibicidoides*, *Globobulimina*, *Uvigerina*) are rare. Calcareous nannofossils (in the 12–8 μm, 8–5 μm, 5–3 μm, and <3 μm fractions) consist of nannoliths (*Discoaster, Sphenolithus*) and coccoliths (e.g. *Helicosphaera*, *Pontosphaera*, *Scyphosphaera*, *Calcidiscus*, *Reticulofenestra*,

Table 2 Quantification of Middle Miocene bulk sediment components (mean values in % based on microscopic observations) and mineralogy (mean values in % based on XRD analysis) from Sites 1006, 1007, 1003, and 1005. Two samples at Site 1006 and one unlithified sample at Site 1007 exhibit very low aragonite abundance compared to others samples. Range of aragonite content without these samples is shown as star for Reference

Bulk		Calcite					Aragonite		Dolomite
Site	Sample induration	Planktonic foraminifera	Calcareous nannofossils	Neritic debris	Macroparticles	Microparticles	Microparticles	Macroparticles	
1006	Unlithified	28% ± 8 (22/42)	46% ± 7 (34/55)	5% ± 2 (2/7)	3% ± 2 (1/7)	5% ± 8 (1/16)	= 87%	12% ± 12 (1/25) (9/25)*	1% ± 1 (0/2)
1007	Unlithified	23% ± 3 (20/27)	45% ± 3 (43/49)	4% ± 1 (3/5)	2% ± 1 (2/3)	5% ± 8 (3/17)	= 79%	19% ± 10 (4/24) (23/24)*	2% ± 1 (1/2)
1007	Lithified	38% ± 7 (29/45)	23% ± 9 (9/29)	11% ± 5 (7/22)	7% ± 2 (5/10)	11% ± 3 (6/16)	= 90%	8% ± 3 (2/12)	2% ± 2 (1/6)
1003	Lithified	22% ± 4 (17/30)	7% ± 5 (0/17)	24% ± 5 (13/30)	16% ± 5 (10/23)	29% ± 8 (19/48)	= 98%	0%	2% ± 2 (0/5)
1005	Lithified	23% ± 2 (19/25)	7% ± 1 (5/10)	21% ± 9 (6/37)	22% ± 7 (11/29)	23% ± 5 (15/32)	= 96%	0%	4% ± 3 (1/11)

±*x*: Standard deviation
(*x*/*y*): (min/max)

Coccolithus). Unspecified biogenic fragments called neritic debris (ranging in size from 5 to 20 μm) are often polycrystalline and always xenomorphic. Their microstructures suggest a biological origin but the specific carbonate-producing organisms could not be identified (Minoletti 2002). Their high magnesium content and their higher abundance at slope sites (Sites 1003 and 1005), however, suggests a neritic origin (Turpin 2006; Turpin et al. 2008).

The second group (macro- and microparticles) refers to all carbonate particles that do not display a distinct biogenic microstructure under the light and the scanning electron microscopes. These particles have been differentiated based on crystallographic, granulometric, and mineralogical criteria: Macroparticles occur in the 20–12 μm, 12–8 μm, and 8–5 μm fractions and consist of calcite, which is mainly xenomorphic and sometimes rhombohedral or dolomite rhombohedra. In contrast, microparticles that are either composed of (1) calcite rhombohedra (<8 μm), which—from a granulometric point of view—are similar to the 'micarb particles' described by Cook and Egbert (1983), Erba (1992) and Mattioli and Pittet (2002), their high proportion in slope sediments and their high magnesium content suggest a bank-top origin (Turpin 2006; Turpin et al. 2008), or of (2) needle-shaped aragonite (<12 μm), which only occurs at distal Sites 1006 and 1007 (Table 2; Fig. 2). Aragonite content increases with decreasing grain size at both sites and correlates with the lithification state of the sediments (Table 3).

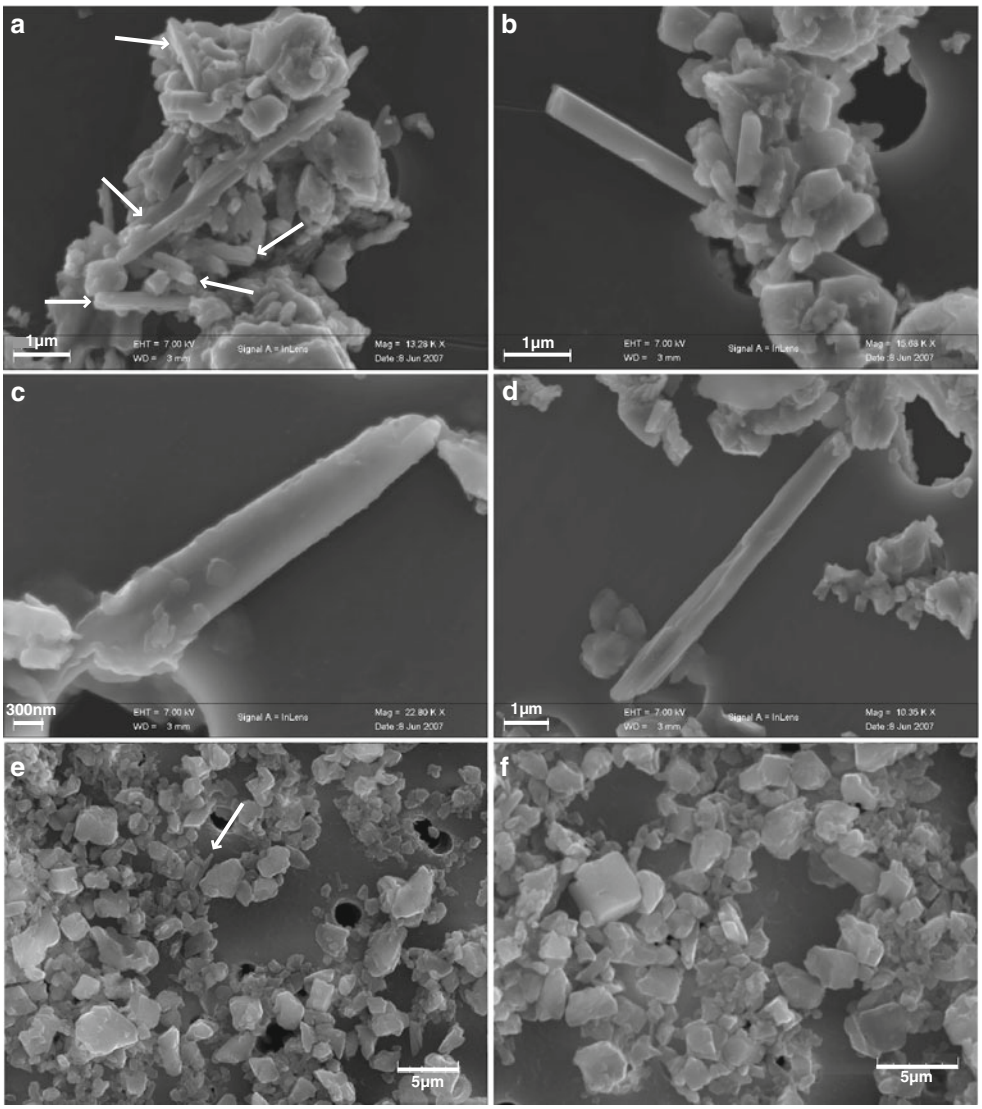

Fig. 2 SEM photomicrographs of <3 μm fractions of Middle Miocene sediments. **a**–**d** Well-preserved aragonite needles of both lithified (**a**, **b**: 27R01–552 mbsf) and unlithified (**c**, **d**: 27R03–554.5 mbsf) samples from Site 1007. **e**, **f** Document the scarcity of aragonite needles in a lithified sample (23R01–591.12 mbsf) at Site 1005. *White arrows* point to aragonite needles

Table 3 Mean aragonite abundance (in %) and Sr content (in ppm) of 12–8 μm, 8–5 μm, 5–3 μm, and <3 μm separated fractions of Middle Miocene sediments from Sites 1006 and 1007 (sixty-eight fractions) depending on the degree of lithification

Fractions (μm)	Site 1006		Site 1007			
	Unlithified sediments		Unlithified sediments		Lithified sediments	
	Aragonite content (%)	Sr content (ppm)	Aragonite content (%)	Sr content (ppm)	Aragonite content (%)	Sr content (ppm)
12–8	7 ± 8 (2/19)	2749 ± 451 (2237/3454)	8 ± 6 (2/13)	2245 ± 564 (1440/2707)	2 ± 1 (1/2)	2724 ± 660 (1785/3833)
8–5	9 ± 7 (2/20)	2848 ± 535 (2301/3840)	13 ± 8 (2/19)	2582 ± 749 (1481/3161)	3 ± 2 (1/7)	2679 ± 562 (1904/3656)
5–3	10 ± 7 (2/20)	2925 ± 421 (2484/3698)	15 ± 8 (4/21)	2891 ± 889 (1567/3459)	5 ± 3 (1/9)	2764 ± 606 (2050/3889)
<3	14 ± 7 (4/21)	3012 ± 548 (2224/3669)	27 ± 14 (6/38)	3512 ± 1242 (1681/4444)	18 ± 6 (8/28)	3571 ± 883 (2345/5041)

±*x*: Standard deviation

(*x*/*y*): (min/max)

At distal sites, the main carbonate sediment components are coccoliths and planktonic foraminifera (74% at Site 1006, 68% and 61% at Site 1007, respectively for unlithified and lithified sediments, Table 2). The microparticles form, on average, 17 and 24% of the unlithified sediments at Sites 1006 and 1007 and 19% of the lithified sediments at Site 1007. Microparticles are mainly composed of aragonite needles in unlithified sediments (12 and 19% at Sites 1006 and 1007), while both calcite (11%) and aragonite (8%) represent microparticles in lithified sediments at Site 1007 (Table 2). The remaining constituents in the carbonate phase at Sites 1006 and 1007 are a mixture of macroparticles and neritic debris. Remaining constituents are more abundant in lithified sediments at Site 1007 (20% on average) than in unlithified sediments at Sites 1006 and 1007 (respectively 9 and 8% on average). The lithified slope sediments at Sites 1003 and 1005 show an entirely different composition (Table 2). At these sites, the pelagic components only account for 29 and 30% of the carbonate phase, respectively. Main constituents are the calcitic microparticles, with mean values of 29 and 23% at Sites 1003 and 1005, while aragonite needles are absent. An important increase in the amount of neritic debris (24% at Site 1003, 21% at Site 1005) and macroparticles (18% at Site 1003, 26% at Site 1005) is also observed.

Carbon and oxygen isotope composition of separated fractions (<12 μm)

Description

The mean isotopic compositions of 72 <12 μm granulometric fractions of the lithified micrites at proximal Sites 1003 and 1005 are given in Table 4. At Sites 1003 and 1005, both oxygen and carbon ratios decrease with decreasing particles size. The isotopic signatures at Site 1003 exhibit higher mean values ($\delta^{18}O = 2.0‰$ and $\delta^{13}C = 2.4‰$) than at Site 1005 ($\delta^{18}O = 1.3‰$ and $\delta^{13}C = 1.8‰$). The isotopic compositions of the <12 μm fractions of Sites 1006 and 1007, where aragonite occurs, have been differentiated according to the location on the transect (Site 1006 vs. Site 1007) and the sediment lithology (unlithified vs. lithified). This enables a distinction between the signature associated with: (1) the unlithified sediments from Site 1006, which display $\delta^{18}O$ values ranging from −0.9 to +0.9‰ and $\delta^{13}C$ varying from +1.1 to +2.5‰, (2) the unlithified sediments from Site 1007, displaying $\delta^{18}O$ values from −0.8 to +1.4‰ and $\delta^{13}C$ ratios from +1.0 to +2.9‰, and (3) the lithified sediments from Site 1007, associated with $\delta^{18}O$ ratios which vary from +0.2 to +1.6‰ and $\delta^{13}C$ values from +1.4 to +2.8‰.

Table 4 Mean $\delta^{13}C$ and $\delta^{18}O$ of 12–8 μm, 8–5 μm, 5–3 μm, and <3 μm fractions and mean value for <12 μm fraction of Middle Miocene lithified sediments from Sites 1003 and 1005 (seventy-two fractions)

Fractions (μm)	Site 1003		Site 1005	
	Lithified sediments		Lithified sediments	
	$\delta^{13}C$ (‰)	$\delta^{18}O$ (‰)	$\delta^{13}C$ (‰)	$\delta^{18}O$ (‰)
12–8	2.5 ± 0.2 (2.2/2.8)	2.1 ± 0.5 (1.2/2.8)	1.9 ± 0.2 (1.6/2.3)	1.4 ± 0.2 (1.1/1.7)
8–5	2.5 ± 0.2 (2.2/2.8)	2.2 ± 0.5 (1.3/2.8)	1.9 ± 0.2 (1.6/2.3)	1.4 ± 0.2 (1.1/1.6)
5–3	2.4 ± 0.2 (2.0/2.7)	2.1 ± 0.5 (1.2/2.7)	1.8 ± 0.2 (1.6/2.1)	1.3 ± 0.2 (1.1/1.6)
<3	2.2 ± 0.2 (1.8/2.5)	1.7 ± 0.4 (0.9/2.3)	1.5 ± 0.1 (1.4/1.8)	1.0 ± 0.2 (0.6/1.2)
Mean composition	2.4 ± 0.3	2.0 ± 0.5	1.8 ± 0.2	1.3 ± 0.3

±*x*: Standard deviation

(*x*/*y*): (min/max)

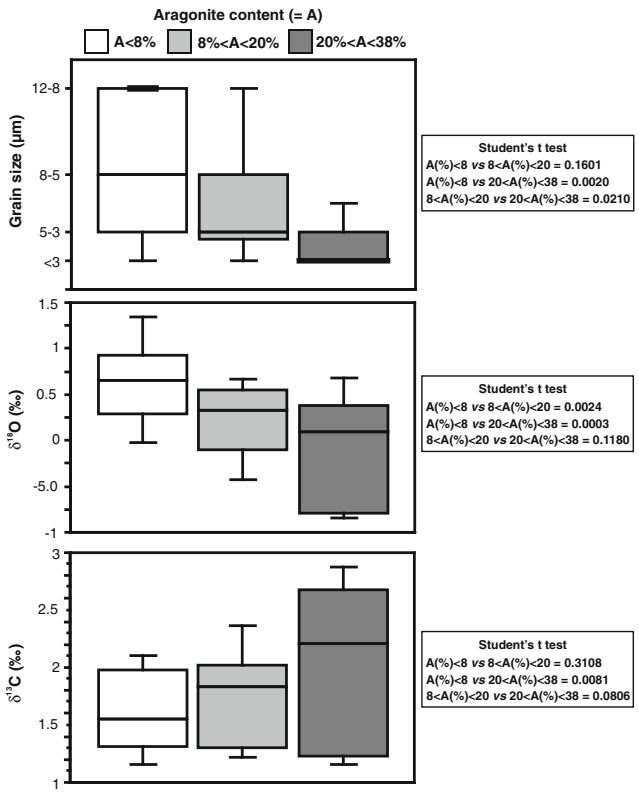

Fig. 3 Grain-size of particles, $\delta^{18}O$ and $\delta^{13}C$ ratios of <12 µm fractions related to the aragonite content clusters (Aragonite < 8%, 8% < Aragonite < 20%, 20% < Aragonite < 38%) at Sites 1006 and 1007 (based on sixty-eight fractions). The *boxes* represent the 25th–75th percentiles (with the median as a *horizontal line*), and the whiskers show the 10th–90th percentiles. The probability values *p*, calculated with the Student's *t*-test, for the three aragonite content clusters are indicated

Interpretation

Statistical analyses performed on the isotopic data and the particle size of the fractions containing aragonite at Sites 1006 and 1007 enable the differentiation of three different clusters of particles based on aragonite content (Student's *t*-test: $p < 0.05$; Figs. 3, 4). Although in some cases, the three clusters are statistically indistinguishable ($p > 0.05$) and display a wide range in the 25th–75th percentiles values, a differentiation between different aragonite clusters is suggested by the median values (Fig. 3). Three clusters are distinguished, while four granulometric-separated fractions for each sample were investigated (12–8 µm, 8–5 µm, 5–3 µm, <3 µm). This can be explained by the distribution of the aragonite needles in the separated fractions. Aragonite abundances of less than 8% correlate with the coarsest 12–8 µm fraction, the aragonite content ranging from 8 to 20% is mostly linked to the 8–5 µm and 5–3 µm intermediate size fractions, and finally, the aragonite content ranging from 20 to 38% is mainly related to the finest <3 µm fraction. The isotopic ratios of each aragonite content cluster, as shown in Fig. 4 and Table 5, are listed according to the site and the lithification state of the sediments.

Strontium content

Description and interpretation

Average strontium content ranges from 2,245 to 3,571 ppm depending on grain size and location of components on the transect (Table 3). In general, for a similar range of aragonite abundance, fractions of lithified sediments of Site 1007 have higher values than unlithified sediments of Sites 1006 and 1007 (Fig. 5). Within unlithified sediments, separated fractions display higher contents at Site 1006 relative to Site 1007 (Fig. 5). Strontium contents are positively correlated to aragonite abundance in <12 µm granulometric fractions (Table 3; Fig. 5).

Discussion

Characterization of diagenetic overprint

C and O stable isotopes signal

Within specific aragonite clusters as present at Site 1007, the separated fractions from lithified intervals are generally enriched in $\delta^{18}O$ and $\delta^{13}C$ and have a lower aragonite content (except for the <3 µm fraction) relative to those from the unlithified intervals at Sites 1006 and 1007 (Tables 3, 5). Frank and Bernet (2000) and Reuning et al. (2002) observed a similar trend in the Miocene bulk sediments at Site 1007. They proposed that the reduced aragonite content is linked to dissolution processes, implying a diagenetic control on the isotopic data of lithified sediments. This early diagenetic overprint is associated with the occurrence of low-magnesium calcite and dolomite rhombohedra in these sediments. In the separated fractions, portions of the calcite macroparticles and all dolomite macroparticles correspond to rhombohedra. Nevertheless, the abundance of dolomite rhombohedra is identical in unlithified and lithified sediments at Site 1007, and calcite macroparticles occur only in slightly higher abundances in lithified intervals compared to unlithified levels at both Sites 1006 and 1007 (Table 2). The abundance of those particles, especially calcitic ones, is also much lower at Sites 1006 and 1007 compared to slope Sites 1003 and 1005 (Table 2) where the diagenetic transformations have been proved to be much more significant (Eberli et al. 1997; Kramer et al. 2000; Swart 2000; Reuning et al. 2002; Swart and Eberli 2005). In addition, the alteration of the aragonite to low-magnesium calcite in GBB sediments

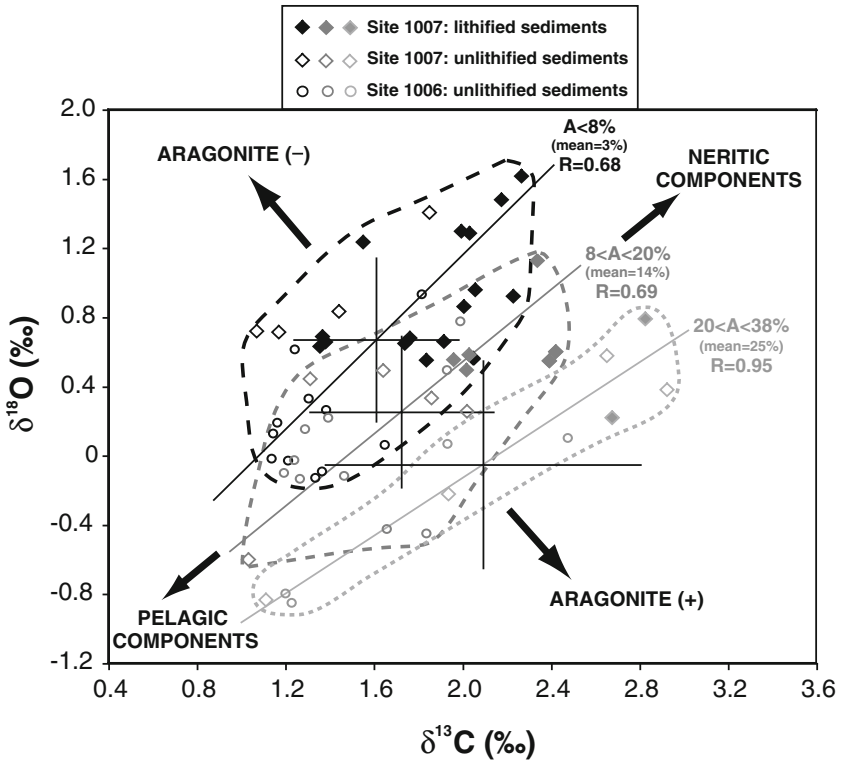

Fig. 4 Carbon and oxygen isotopic composition of <12 μm fractions of Middle Miocene sediments at Sites 1006 and 1007 (based on sixty-eight fractions). Values are differentiated depending on the location on GBB transect, sediment lithification, and aragonite abundance. Unlithified sediments from Sites 1006 and 1007 are indicated by open circles and diamonds, respectively, while filled diamonds represent lithified sediments from Site 1007. The first aragonite cluster (aragonite content < 8%) is represented by a *dashed line* and *symbols* in black, the second aragonite cluster (8% < aragonite content < 20%) by a *dashed line* and *symbols* in *dark grey*, and the third aragonite cluster (20% < aragonite content < 38%) by a *dashed line* and *symbols* in *light grey*. Linear trends (reduced major axis) with their coefficient of determination *R* and error bars, representing the coefficient of variation (CV), are presented for each aragonite cluster

occurs during closed system conditions resulting in a limited influence on carbonate $\delta^{13}C$ composition (Swart 2002; Swart and Eberli 2005).

Previous studies (Frank and Bernet 2000; Reuning et al. 2002) have focused their analysis on bulk sediments, representing an admixture of primary and diagenetic phases. In this study, samples have been disaggregated, and analyses were performed on particular size fractions separating primary from secondary (authigenic) particles. In addition, at Site 1007, small-sized particles such as skeletal components (coccoliths) and aragonite needles (Fig. 2) show no evidence of secondary overgrowth in both lithified and unlithified intervals. Therefore, the isotopic data of <12 μm fractions from Site 1007 are considered to represent a better approximation of primary geochemical values relative to those from bulk sediments. Dissolution–recrystallization processes that have a limited effect on carbon isotope ratios and a moderate effect on oxygen ratios potentially affect lithified sediments at Site 1007. This may explain the occurrence of rhombohedra in a slightly higher proportion in those intervals. In summary, the elevated carbon-isotopic composition of the lithified sediments at Site 1007 is interpreted to represent the original seawater $\delta^{13}C_{DIC}$.

In contrast, ^{18}O-enriched values of <12 μm fractions measured from lithified sediments at Sites 1003 and 1005 (Table 4) are likely to record, at least in part, an early diagenetic overprint. Evidence for this includes higher numbers of calcite and dolomite rhombohedral macroparticles (Table 2) as opposed to sediments at Sites 1006 and 1007 (unlithified and lithified).

Strontium content

From the modern carbonate platforms of Belize, Gischler and Zingeler (2002) have shown that the <4 μm mud fraction exhibit lower Sr values compared to the 20- to 4-μm muds. These authors assume that this difference could be linked to more effective early recrystallization processes, leading to a loss in strontium, within smaller components. In the case of the samples analysed here, this phenomenon seems unlikely due to the increase in Sr

Table 5 Mean $\delta^{13}C$ and $\delta^{18}O$ of each aragonite content cluster of <12 μm fraction of Middle Miocene sediments from Sites 1006 and 1007 (sixty-eight fractions) depending on the degree of lithification

<12 μm fraction	Site 1006		Site 1007				Mean		
Aragonite domain (%)	Unlithified sediments		Unlithified sediments		Lithified sediments		Compositions		
	$\delta^{13}C$ (‰)	$\delta^{18}O$ (‰)	$\delta^{13}C$ (‰)	$\delta^{18}O$ (‰)	$\delta^{13}C$ (‰)	$\delta^{18}O$ (‰)	Aragonite (%)	$\delta^{13}C$ (‰)	$\delta^{18}O$ (‰)
<8	1.3 ± 0.2 (1.1/1.8)	0.2 ± 0.3 (−0.1/0.9)	1.4 ± 0.3 (1.1/1.9)	0.9 ± 0.3 (0.7/1.4)	1.9 ± 0.3 (1.4/2.3)	0.9 ± 0.4 (0.5/1.6)	3 ± 2	1.6 ± 0.4	0.7 ± 0.5
8–20	1.5 ± 0.3 (1.2/2.0)	0.0 ± 0.4 (−0.4/0.8)	1.6 ± 0.4 (1.0/2.0)	0.2 ± 0.4 (−0.6/0.5)	2.2 ± 0.2 (2.0/2.4)	0.6 ± 0.2 (0.5/1.1)	14 ± 4	1.7 ± 0.4	0.2 ± 0.4
20–38	1.7 ± 0.6 (1.2/2.5)	−0.4 ± 0.5 (−0.8/0.1)	2.2 ± 0.8 (1.1/2.9)	0.0 ± 0.6 (−0.8/0.6)	2.8 ± 0.1 (2.7/2.8)	0.5 ± 0.4 (0.2/0.8)	25 ± 7	2.1 ± 0.7	−0.1 ± 0.6

±*x*: Standard deviation
(*x*/*y*): (min/max)

content (and aragonite abundance) with decreasing component grain sizes (Table 3; Fig. 5).

Surprisingly, fractions of lithified sediments at Site 1007 have higher Sr contents, while these intervals were slightly more affected by early diagenesis relative to unlithified intervals. Traces (<2%) of Ba-rich celestite ($SrxBa(1-x)SO_4$) have been found in the Middle Miocene samples at Sites 1006 and 1007 (Eberli et al. 1997; Turpin 2006; Turpin et al. 2008). The local dissolution of aragonite is probably the Sr2+ source for celestite formation (Reuning et al. 2002), which might affect Sr contents. However, celestite is only found in unlithified intervals (Reuning et al. 2002), or its abundance is slightly higher in unlithified rather than in lithified levels (Turpin 2006). Therefore, Sr content seems to be mainly related to the variation of aragonite abundance in the <12 μm fractions without being affected by early diagenetic processes. Nevertheless, it is here acknowledged that a detailed understanding of the higher Sr values in lithified sediments is lacking.

Palaeo-environmental record by the mineralogy and the type of fine-grained particles: an isotopic approach

Isotopic signatures and aragonite contents of the <12 μm granulometric fractions at Sites 1006 and 1007 are strongly correlated (Figs. 3, 4; Table 5). An increase in the aragonite content is positively correlated with $\delta^{13}C$ and negatively correlated with $\delta^{18}O$. Pelagic particles (coccoliths) form the main calcite portion in the separated fractions of unlithified sediments at Sites 1006 and 1007. In contrast, neritic debris and calcitic microparticles (identified as neritic-origin particles; Turpin 2006; Turpin et al. 2008) form the main calcite portion in the fractions of lithified sediments at Site 1007. In samples dominated by pelagic components, more depleted $\delta^{18}O$ and $\delta^{13}C$ values are found while isotopic ratios are more positive in samples characterized by a calcitic fraction mainly composed of neritic components (Fig. 4).

Carbon isotope ratios

Several studies showed that positive correlations exist between $\delta^{13}C$ and aragonite content at carbonate platforms, e.g. the Bahamas (Weber 1967; Swart and Eberli 2005; Swart et al. 2009), Australia (Weber and Woodhead 1969; Dix et al. 2005), and selected places at Belize, Maldives, and Kuwait (Gischler et al. 2009). The origin of the ^{13}C-enriched values of aragonite on GBB is not well understood. Higher isotope values are in part explained by the fact that calcite and aragonite have different equilibrium isotopic fractionations with respect to seawater. Consequently, aragonite is enriched by approximately 1 ‰ in

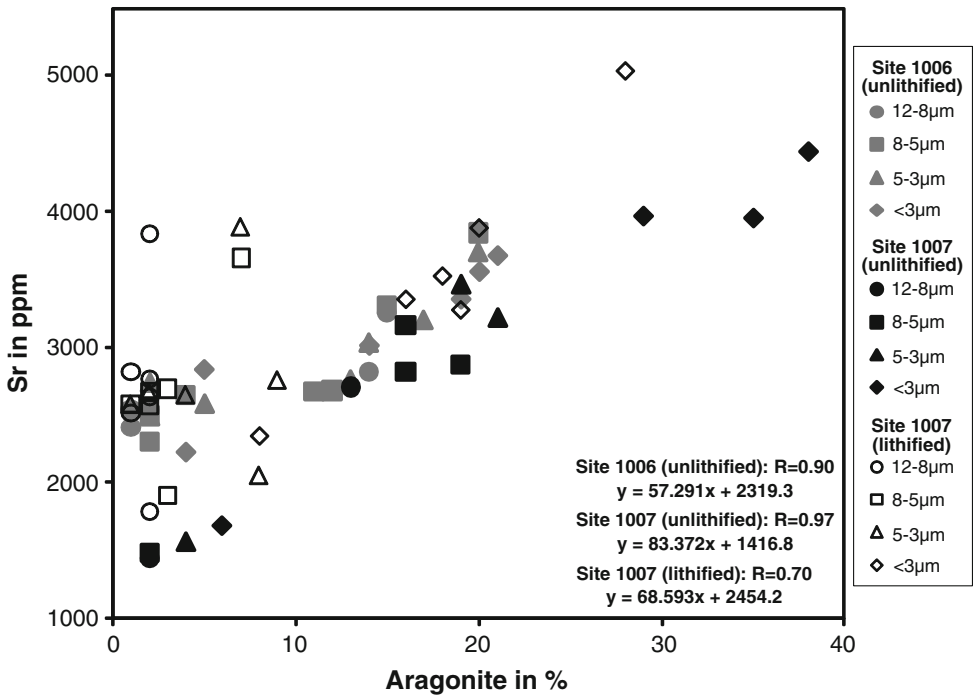

Fig. 5 Aragonite abundance related to Sr concentrations in the 12–8 µm, 8–5 µm, 5–3 µm and < 3 µm fractions of Middle Miocene sediments at Sites 1006 and 1007. Linear trend equations with their correlation coefficients *R* are indicated

$\delta^{13}C$ relative to calcite (Emrich et al. 1970; Turner 1982; Gonzalez and Lohmann 1985). The $\delta^{13}C$ ratios of shallow-water sediments deposited on the modern GBB, which are essentially 100% aragonite (Reijmer et al. 2009), lie between +4 and +5‰ (Lowenstam and Epstein 1957; Shinn et al. 1989; Swart and Eberli 2005), whereas the $\delta^{13}C$ values of modern low-magnesium calcite coccoliths range between 0 and +1‰ (Milliman 1974). In addition, $\delta^{13}C$ is also influenced by seawater $\delta^{13}C_{DIC}$. The elevated $\delta^{13}C$ of the GBB modern sediments is perhaps also explained by a high seawater $\delta^{13}C_{DIC}$ due to fractionation during photosynthesis (preferential removing of ^{12}C causing an enrichment of waters in ^{13}C; Immenhauser et al. 2008; Swart et al. 2009). For this reason, organic or inorganic carbonates formed in the shallow realms of Great Bahama Bank tend to record higher $\delta^{13}C$ values than carbonates precipitated in the open ocean (Swart and Eberli 2005). This relation might explain the higher Miocene $\delta^{13}C$ ratios of fractions enriched in aragonite and fractions enriched in calcitic neritic particles (Fig. 4). Similarly, elevated $\delta^{13}C$ ratios might also suggest a shallower seawater environment for the precipitation of aragonite. It is, therefore, concluded that the mineralogy and the relative proportion of pelagic and neritic material in Middle Miocene micritic sediments affect the $\delta^{13}C$ signature of samples along the GBB transect.

Oxygen isotope ratios

Calcite and aragonite have different equilibrium isotopic fractionations with respect to seawater. The difference in fractionation factors between these two minerals is expected to lead to a shift towards ^{18}O-enriched values in aragonite-rich fractions (Tarutani et al. 1969; Gonzalez and Lohmann 1985). In contrast to this, a decrease of $\delta^{18}O$ is observed with increasing aragonite abundance (Fig. 4; Table 5). Reuning et al. (2002) documented that Miocene unlithified intervals at Site 1007, enriched in aragonite, display lower $\delta^{18}O$ ratios compared to lithified intervals as is the case for the Miocene-separated fractions shown in this study (Fig. 4). Reuning et al. (2002) explained this discrepancy as a perturbation of aragonite $\delta^{18}O$ compared to calcite $\delta^{18}O$ due to diagenesis. However, as discussed before, the $\delta^{18}O$ record of the separated fractions is only moderately influenced by diagenesis. This implies that fluctuations in $\delta^{18}O$, as obtained from the analysis of specific fractions, are more likely to record seawater environment during precipitation of carbonate particles as opposed to diagenetic signature or mineralogical artefact resulting from different isotopic fractionation factors with respect to seawater. The depleted $\delta^{18}O$ composition of separated fractions showing higher aragonite content implies that aragonite $\delta^{18}O$ reflects precipitation under higher seawater temperature conditions. This evidence, combined with higher $\delta^{13}C$ ratios, strongly suggests deposition under shallow (bank top) seawater conditions.

Particles from the deeper basinal Site 1006 display more negative compositions compared to the signature of the particles from the toe-of-slope Site 1007 (Fig. 4; Table 5). This relationship implies that these values represent fluctuations of seawater $\delta^{18}O_w$, linked to the modifications of seawater salinity, rather than seawater

temperature. This observation is in agreement with Cloud (1962a), Lowenstam and Epstein (1957), and Shinn et al. (1989), who all have shown an increase in seawater salinity from west to east across modern GBB. The relationship between $\delta^{18}O_w$ and salinity on GBB is rather complex but Lowenstam and Epstein (1957), Shinn et al. (1989) as well as Swart et al. (2009) suggested an overall positive correlation between $\delta^{18}O_w$ and seawater salinity. Particles from unlithified sediments taken at the distal Site 1006 and the toe-of-slope Site 1007, dominated by pelagic components, record lower seawater salinity than particles from lithified sediments at the toe-of-slope Site 1007 dominated by neritic constituents. From this, it is concluded that the differences in oxygen-isotopic composition between the distal Site 1006 and the toe-of-slope Site 1007 reflect seawater salinity distribution from west (basin) to east (toe-of-slope) and are comparable both for the Middle Miocene ramp as for the modern flat-topped platform of Great Bahama Bank. Furthermore, $\delta^{18}O$ values measured at Sites 1006 and 1007 reflect a combination of seawater temperature and salinity effects. Seawater temperature is recorded by aragonite versus calcite particles, and seawater salinity is recorded by pelagic versus neritic components in the calcitic fraction.

The different seawater isotopic characteristics recorded at Sites 1006 and 1007 and the variations in fraction composition (mineralogy and components), related to these variable isotopic signatures, also explain the wide range of the percentiles values and, in some cases, the lack of clear trends in these data (Fig. 3).

At Sites 1003 and 1005, positive $\delta^{18}O$ ratios (Table 4) relative to Sites 1006 and 1007 also relate to the type of components in the fractions (calcite and dolomite rhombohedral macroparticles and neritic particles). The high amount of neritic debris, relative to lithified levels of Site 1007 (Table 2), likely implies that portions of the resulting oxygen-isotopic signal might also record the seawater salinity, as in lithified levels at Site 1007. This suggests that a primary signal, here seawater salinity, is recorded by neritic particles and an early diagenetic overprint is recorded in rhombohedral macroparticles.

Isotopic ratios of the middle slope Site 1003 display higher values compared to the upper slope Site 1005. This feature could be explained by a differential diagenetic alteration in the middle slope domain relative to the upper slope domain as suggested in other studies dealing with the geochemistry of carbonate slope settings (van der Kooij et al. 2009). Alternatively, if elevated oxygen isotope ratios represent seawater salinity, then higher seawater salinities must be assumed for the middle slope Site 1003 ($\delta^{18}O_{mean} = +2‰$) relative to the upper slope Site 1005 ($\delta^{18}O_{mean} = +1.3‰$). This assumption seems unlikely due to the west to east salinity distribution on GBB. This discrepancy is perhaps best explained by the higher amount of turbiditic intervals at Site 1003 (Eberli et al. 1997; Bernet et al. 2000). The bulk of the bank-top material, recording higher seawater salinities and transported downslope by gravity currents, bypasses Site 1005 and mainly settles at Site 1003. Lithified levels of Site 1007, showing higher abundance of neritic-origin particles related to higher $\delta^{18}O$ ratios compared to the unlithified levels of Sites 1006 and 1007, have been associated with the finest part of turbiditic intervals that deposited their main sediment load at Site 1003 (Turpin et al. 2008).

In conclusion, the complexity of a multi-parameter system including mineralogy, seawater temperature, seawater salinity, sediment transport and re-deposition and finally diagenesis is a limiting factor for the interpretation of geochemical data. Nevertheless, the fractionation-specific analysis of carbonate particles from spatially and bathymetrically separated localities on the Middle Miocene Great Bahama Bank sheds light on the relative significance of specific parameters that affect the isotopic composition of bulk samples.

Aragonite needles: Precipitation site

Aragonite needles occur in the distal Middle Miocene pelagic sediments (Sites 1006 and 1007) of the western GBB transect, while they are absent in the proximal realm (Sites 1003 and 1005; Fig. 2). This might suggest that they are predominantly precipitated and deposited in a pelagic environment. The only biological planktonic aragonite source conceivable is from the fragmentation of pteropods. However, the needle shape of the aragonite (van der Spoel 1976; Lalli and Gilmer 1989) excludes this source. In contrast, this needle shape of aragonite has been extensively described in the literature as being characteristic of modern, shallow-water environments in the Bahamas (Ginsburg 1956; Lowenstam and Epstein 1957; Purdy 1963a, b; Mathews 1966; Stockman et al. 1967; Neumann and Land 1975; Wilber et al. 1990; Macintyre and Reid 1992). Furthermore, Miocene aragonite-rich fractions exhibit ^{13}C-enriched and ^{18}O-depleted ratios suggesting a precipitation in a shallow environment. Finally, the strontium content of Miocene <12 μm fractions, representing a mean aragonite content of only 12% in bulk samples at Sites 1006 and 1007, display high values (Table 3), similar to high-strontium content of pure aragonite from the modern Bahamian bank. In contrast, pteropod-derived aragonite, as it is the case for all gastropods, is characterized by mean Sr values of 1,000 ppm (Kinsman 1969; Milliman 1974). All aforementioned arguments favour aragonite needle precipitation on the shallow, proximal Middle Miocene Great Bahama Bank and subsequent transport to distal Sites 1006 and 1007.

Aragonite needles: mode of transportation

The production of the Middle Miocene aragonite needles in the shallow-water environment of GBB and their occurrence at distal sites suggest an allochtonous origin and imply basinward transport. These fine-grained particles could be exported from the bank either in suspension or by gravity currents. In the latter case, aragonite needles might be linked to the distal part of turbidite deposits, which concentrate the finest particles. However, the absence of aragonite needles at the proximal sites, their small size and their well-preserved morphology (Fig. 2) support suspension-driven transport. It thus seems likely that Middle Miocene off-bank transport of aragonite needles occurred in a similar way as the present-day sediment export processes on the Bahamas (McCave 1972; Neumann and Land 1975; Schlager and Chermak 1979; Droxler and Schlager 1985; Heath and Mullins 1984; Shinn et al. 1989; Wilber et al. 1990; Wilson and Roberts 1992, 1995; Rendle-Bühring and Reijmer 2005). Next to storms and hurricanes, which occasionally may cause aragonite export, long-term fine-grained sediment transport patterns from this production zone are related to the wind-driven surface currents (Roth and Reijmer 2005). On the bank, needles also may serve as nuclei for further aragonite precipitation if the seawater chemical conditions are favourable (Roth and Reijmer 2005). Once transported off-bank, the aragonite needles are exported as suspended material towards the leeward escarpment.

Present-day Bahamian off-bank sediment transport occurs almost exclusively during sea-level highstands when the platform top is flooded, implying high carbonate production rates (Droxler and Schlager 1985; Austin et al. 1988; Schlager et al. 1994; Eberli et al. 1997; Betzler et al. 1999). Conversely, in the Miocene carbonate ramp, the production area was not significantly reduced during sea-level lowstand due to downstepping along the gentle ramp topography (Burchette and Wright 1992; Schlager et al. 1994). Consequently, the ramp morphology might favour needles export during both sea-level highstands and lowstands (Bernet et al. 2000; Swart and Eberli 2005; Turpin et al. 2008). The absence of aragonite needles at the proximal part of the slope implies granulometric sorting. Previous authors, however, postulated that pore fluid circulation inside the bank is preferentially active in permeable sediments in the slope domain (Eberli et al. 1997; Caspard et al. 2004). For this reason, the absence of needles in the proximal sites is certainly enhanced by aragonite dissolution processes resulting in precipitation of diagenetically more stable authigenic carbonates.

Aragonite needles: mode of precipitation

An ongoing debate regarding the origin of Recent Bahamian aragonite needles alternatively considers a skeletal origin (codiacean algae fragmentation; Neumann and Land 1975), a spontaneous precipitation from seawater (Cloud 1962a, b; Bathurst 1975) or a whiting-related origin (Broecker and Takahashi 1966; Morse et al. 1984; Robbins and Blackwelder 1992; Robbins et al. 1997; Yates and Robbins 1999; Broecker et al. 2000). Obviously, the same problem relates to the origin of Middle Miocene aragonite needles. In order to contribute to this debate, isotopic evidence (Fig. 6) here is used for comparison. The data considered include:

1. Codiacean algae (*Halimeda*, *Penicillus*, *Udotea*) of recent shallow marine environments ($\delta^{18}O$ values between -0.8 and $-4‰$ and $\delta^{13}C$ values between -1 and $+8‰$) and more precisely Bahamian *Halimeda* isotopic composition (from -1.4 to $-3.8‰$ and from $+0.8$ to $+8‰$ for $\delta^{18}O$ and $\delta^{13}C$, respectively) from Lee and Carpenter (2001).
2. Isotopic values from modern Bahamian inorganically precipitated aragonite. The $\delta^{18}O$ range of aragonite (from -1.2 to $+0.8‰$) formed at equilibrium with GBB surface waters was calculated by Swart et al. (2009) using the palaeo-temperature equation of Epstein et al. (1953). They assumed a mean GBB sea surface temperature value of 25°C and a range of GBB $\delta^{18}O_w$ from $+0.75$ to $+2.93‰$ SMOW. The range of $\delta^{13}C$ (from $+2.6$ to $+5.8‰$) for aragonite precipitated at equilibrium with GBB surface waters ($\delta^{13}C_{DIC}$ varying from $+0.4$ to $+2.4‰$) is reported in Swart et al. (2009).
3. Modern Bahamian whitings particles are characterized by mean aragonite content of 86% and display $\delta^{18}O$ ratios between -0.2 and $+0.9‰$ and $\delta^{13}C$ values between $+4.1$ and $+5.8‰$ (Shinn et al. 1989). The isotopic composition of particles precipitated during whiting events included within the inorganic aragonite domain implies equilibrium precipitation with seawater.
4. Middle Miocene <12 μm separated fractions (Fig. 4) as reported in this study are equally significant. In order to compare the Middle Miocene isotopic ratios with those of modern algae, inorganic aragonites, and whiting-related precipitates, a glacial effect correction has been applied on the Middle Miocene $\delta^{18}O$ values. The isotopic composition of the oceans prior to the formation of the presently existing ice sheets has been estimated by Shackleton and Kennett (1975) at $-1.2‰$ expressed in relation to the PDB standard. The Miocene carbonates investigated overlap in age with the Middle–Late Miocene transition period marked by a more permanent and stable character of the Antarctic ice sheets. For this reason, a glacial effect range has been considered. The comparison between the values of the Middle Miocene period and the Plio-Pleistocene

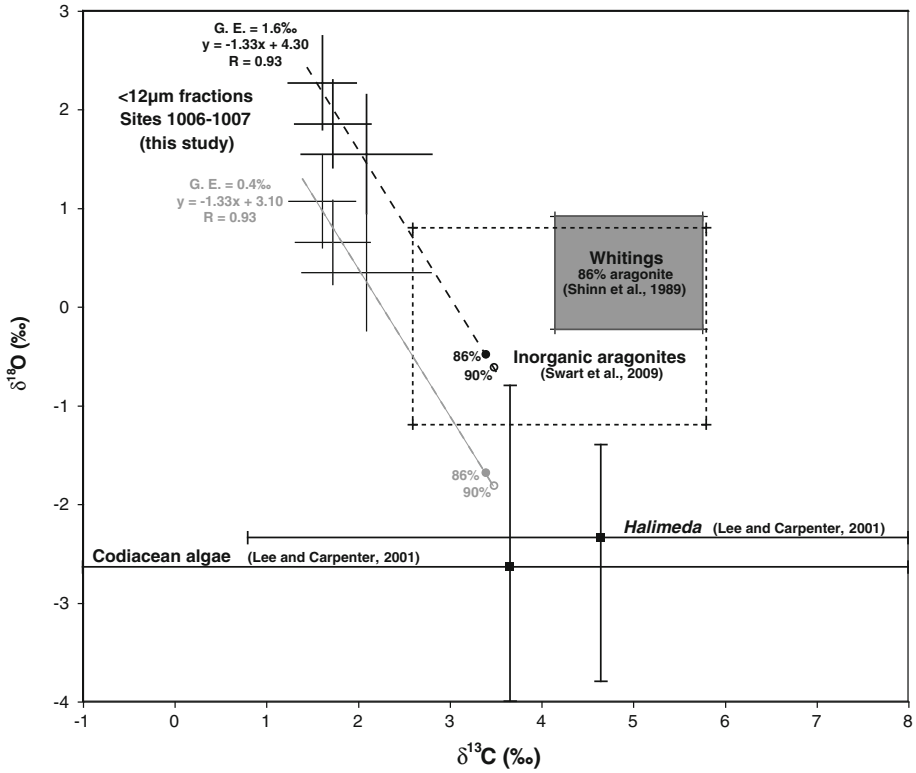

Fig. 6 Comparison of carbon and oxygen isotopic composition of modern codiacean algae and Bahamian *Halimeda* (Lee and Carpenter 2001; *filled squares* represent the mean values, and *errors bars* represent the range of values); Present-day Bahamian inorganic aragonites (Swart et al. 2009) and modern Bahamian whiting-related precipitates (Shinn et al. 1989); and the mean isotopic signature of the < 12 µm fractions of Middle Miocene sediments at Sites 1006 and 1007 (present study). The three aragonite clusters (aragonite < 8%, 8% < aragonite < 20%, 20% < aragonite < 38%) previously defined in Fig. 4 are shown. Glacial effect (G.E.) corrections have been applied on the $\delta^{18}O$ of the aragonite clusters: in grey G.E. = 0.4‰, in black G.E. = 1.6‰. *Error bars* represent corrected coefficients of variation of each aragonite cluster. The theoretical isotopic signatures corresponding to aragonite contents of 86 and 90% are indicated

values in the long-term $\delta^{18}O$ curve of Zachos et al. (2008) is used to apply a range from +0.4 to +1.6‰ on Middle Miocene $\delta^{18}O$. Thus, after correction, $\delta^{18}O$ ratios display values from −0.4 to +2.0‰ for a glacial effect of +0.4‰ and from +0.8 to +3.2‰ for a glacial effect of +1.6‰.

The mean aragonite content of the modern Bahamian whiting-related particles is 86% (Shinn et al. 1989), and the aragonite needles represent up to 85–90% of the modern fine sediments of the Bahamian banks (Milliman 1974; Heath and Mullins 1984). A direct isotopic analysis of the aragonite of individual Miocene granulometric fractions could not be made because of the limited amount of this mineral in the fractions analysed (maximum of 38%, Table 3; Fig. 4). Therefore, in order to compare the isotopic results from the separated fractions, a linear regression analysis has been applied in order to calculate two theoretical aragonite isotopic signals related to aragonite contents of 86 and 90%, respectively. For the $\delta^{18}O$, if the glacial effect is equal to 0.4‰, then the equation is: $\delta^{18}O = -0.0328 \times \%\text{Aragonite} + 1.1461$, and if the glacial effect is equal to 1.6‰, then the equation is: $\delta^{18}O = -0.0328 \times \%\text{Aragonite} + 2.3461$ ($R = 0.9960$). For the $\delta^{13}C$, the equation is: $\delta^{13}C = -0.0219 \times \%\text{Aragonite} + 1.5049$ ($R = 0.9567$). These calculated oxygen and carbon isotopic compositions display an intermediate signature between the codiacean algae and the whitings signatures (Fig. 6). Considering a glacial effect of +1.6‰ on Middle Miocene values, aragonite isotopic composition tends to agree with values obtained from whiting-related particles. For a glacial effect of +0.4‰, the aragonite signature lies close to the codiacean algae domain. This record thus suggests that the Middle Miocene aragonite needles consist of an admixture of codiacean algae and particles derived from whitings.

Previous workers (Kinsman 1969; Milliman 1974; Loreau 1982; Milliman et al. 1993; Gischler and Zingeler 2002) have used Sr contents to differentiate inorganically precipitated aragonite from algal aragonite. Inorganic aragonite is considered to contain 9,500–10,000 ppm Sr, while aragonite produced by codiacean algae is characterized by Sr contents ranging from 8,000 to 9,000 ppm.

For comparison, theoretical Sr concentrations have been calculated. These concentrations, related to aragonite contents of 86 and 90%, are based on linear regression equations linking the Sr content and the abundance of aragonite (Fig. 5). For the unlithified sediments of Site 1006, theoretical Sr contents are equal to 7,250 and 7,475 ppm, for the unlithified sediments of Site 1007 to 8,590 and 8,920 ppm and for the lithified sediments of Site 1007 to 8,355 and 8,630 ppm, for 86 and 90% of aragonite, respectively. These theoretical values do not reached 9,000 ppm and may well indicate that Middle Miocene aragonite needles are linked to an algal source.

Middle Miocene aragonite needles mainly occur in <3 μm fractions (Table 3). Under SEM (Fig. 2), individual needles are lath-shaped with rounded edges, exhibit irregular outlines and terminate gradually (rarely abruptly). Macintyre and Reid (1992) and Shinn et al. (1989) have shown that modern aragonite crystals in whitings (as in Bahamian bottom sediments) are typically stubby, bladed crystals, <4 μm long, with irregular outlines and pointed terminations. In contrast, the algal needles are generally larger (mostly 3–10 μm long) and characteristically occur as six-sided prisms with 2-fold monoclinic symmetry, sharp crystals faces, and blunt terminations (Macintyre and Reid 1992). Macintyre and Reid (1995) have also shown on *Halimeda incrassata* specimens that aragonite can exhibit three types of crystals. The original skeletal elements are 1- to 3-μm aragonite needles, characterized by flat to slightly rounded ends. Within living plants, these needles can be altered to anhedral equant aragonite 0.1–0.5 μm in size (called 'minimicrite'). Finally, large euhedral crystals, typically 6–12 μm long, may be precipitated during a late stage of calcification of *Halimeda*. The anhedral crystals, due to their shape, can be excluded in explaining the origin of Middle Miocene aragonite needles. The original algal needles exhibit similar size as the Middle Miocene needles, however, the differences in symmetry, terminations, and outlines enable to reject this origin. One crystal specimen could be related to an algal origin (Fig. 2b), in particular to a large euhedral crystal, due to its larger size (around 6 μm in length), its flat termination and its regular outlines. However, SEM observations indicate that these crystals are rare in the Middle Miocene aragonite-rich fractions. In modern shallow-water environments, euhedral crystals generally constitute less than 20% of the total carbonate in a thallus (Macintyre and Reid 1995). By analogy, euhedral crystals should thus represent only a small part of Miocene aragonite needles. In addition, on the present-day GBB platform, morphological analysis of aragonite indicates that only a small part of Bahamian needles (from 5 to 25%) result from the fragmentation of codiacean algae (Cloud 1962a, b; Bathurst 1975, Loreau 1982; Shinn et al. 1989; Milliman et al. 1993). Needles constitute only 25–40% of many of the calcareous green algae, and most of the aragonite exists as equant nanograins (Loreau 1982; Macintyre and Reid 1992, 1995). In Miocene sediments, Reuning et al. (2002) observed very low abundances of *Halimeda* needles along the GBB transect. Finally, the morphology of the Middle Miocene aragonite needles (size, shape, terminations, and outlines) mostly corresponds with the properties found in whiting-related needles. Therefore, geochemical and morphological evidences imply that Middle Miocene aragonite needles are in part the result of algal fragmentation but predominantly relate to whiting phenomena.

Preconditions for whiting-related precipitation in a carbonate ramp setting

Precipitation during whiting events results on average in 10-mg particles per 1 l of seawater with concentrations as low as 1.5 mg/l in the water masses surrounding whiting areas. Whitings are sudden features and can persist for several days or several weeks before the carbonate particles in suspension settle to the seafloor (Shinn et al. 1989). These particles would form the main part of the fine-grained carbonate particles (<5 μm) of sediments (Thompson et al. 1997). The whiting-related particles themselves and the seawater composition have been studied in situ during whiting events (Cloud 1962a, b; Wells and Illing 1964; De Groot 1965; Broecker and Takahashi 1966; Neev and Emery 1967; Shinn et al. 1989). Resulting analyses have been variably interpreted. Wells and Illing (1964) proposed that whitings correspond to a precipitation of aragonite from seawater, while others have suggested that this phenomenon is linked to sediment re-suspension (De Groot 1965; Neumann and Land 1975) by bottom-feeding fish, boats, or storms/ocean currents. The bottom sediment re-suspension hypothesis is supported by radiocarbon dating of whitings precipitates resulting in an age consistent with the radiocarbon age of the underlying sediments (Broecker and Takahashi 1966; Morse et al. 1984; Broecker et al. 2000). Less than 15% of whitings precipitates correspond to recent carbonate material (Broecker et al. 2000). Numerous authors (Cloud 1962a, b; Wells and Illing 1964; Shinn et al. 1989; Thompson 2000), however, question the bottom-feeding fish hypothesis because clear water masses have been observed beneath whitings, excluding a re-suspension mechanism. Shinn et al. (1989) proposed that whitings are more likely a combination of bottom sediment re-suspension and direct precipitation. Nevertheless, a bio-induced precipitation triggered by picoplankton is favoured by many authors (Thompson and Ferris 1990; Robbins and Blackwelder 1992; Robbins et al. 1996; Thompson et al. 1997; Yates and Robbins 1999; Thompson 2000; Sondi and Juračič 2010).

Modern observations on the spatial distribution of whiting events show that these features are not randomly distributed but predominantly occur on the north central part of GBB (Robbins et al. 1997), i.e. near the position of the current study area. Furthermore, morphological characteristics of Middle Miocene aragonite needles suggest that they predominantly result from whiting-related precipitation. It therefore seems likely that the whitings were also a common feature of water masses covering the Middle Miocene ramp.

At present, direct precipitation of aragonite occurs on the platform with peak occurrences in April and October (Tao 1994; Robbins et al. 1997). Aragonite precipitates when environmental conditions are most favourable due to higher water temperatures and a high level of seawater over-saturation with respect to aragonite relative to the surrounding open ocean (Demicco and Hardie 2002). Therefore, aragonite production on the modern GBB is considered to be dependent on water depth, distance from the platform margin, and residence time of the water masses on the platform (Broecker and Takahashi 1966; Demicco and Hardie 2002). These parameters have an impact on the aragonite saturation state of the platform waters, a parameter which is of major importance for aragonite precipitation (Morse and Mackenzie 1990; Duan and Sun 2003).

Morphological characteristics and, to a minor extent, isotopic ratios of Middle Miocene aragonite provide evidence of a whiting-type precipitation along the GBB ramp profile, although the Miocene ramp morphology allows for a better water exchange with open ocean water masses compared to the modern rimmed platform (Betzler et al. 1999; Swart and Eberli 2005). The high Miocene carbonate saturation in aragonite might occur because this geological time interval, as the Plio-Pleistocene, corresponds to an aragonite sea mode (Sandberg 1975; Stanley and Hardie 1998). In addition, whitings have also been observed on modern ramp settings such as the shelves of Yucatan (Belize) or the shallow region of the Persian Gulf. The sedimentary significance of whitings observed in the southwest of Cay Corker in Belize is unknown, although the water column is supersaturated with respect to aragonite (Purdy and Gischler 2003). In the Persian Gulf, Wells and Illing (1964) have shown that whiting formation, most frequent in its southern part, is not accompanied by salinity or temperature variations or by changes in seawater pH. The production of large quantities of aragonite needles in the Persian Gulf is also largely independent of water depth. In the Persian Gulf, however, the needles tend to be smaller in size and occur very frequently in water depths of less than 10 m, whereas aragonite needles are larger and less frequent in water depths down to approximately 30 m.

Wells and Illing (1964) argued that whitings form as a result of CO_2 uptake by phytoplankton bloom because they observed an increase in the phytoplankton population in water samples during whiting events. In the modern GBB, whitings have also been linked to sudden blooms of unicellular organisms resulting from epicellular precipitation of calcium carbonate (Robbins and Blackwelder 1992; Yates and Robbins 1995, 1999; Thompson et al. 1997; Thompson 2000). Tyrrell and Merico (2004) suggested that the bloom of modern unicellular algae (*E. huxleyi*) could also occur in open marine environments. This is because this process is driven by a combination of factors (abundant light, low silicate, high N/P ratios, low dissolved carbon dioxide, and high carbonate saturation state) and not only by temperature and salinity. These considerations are in agreement with the previous work of Wells and Illing (1964) in the Persian Gulf.

In the modern Bahamas, Dierssen et al. (2009) linked whitings formation to a re-suspension of sediments due to a wind-driven oceanic circulation (Langmuir cells). This circulation, occurring in the shallow-water environment, is caused by the interaction between wind-driven shear current and the Stokes drift current from gravity waves (Thorpe 2004). This type of oceanic circulation is also envisaged for the shallow-water environment of the Miocene ramp context, depending only on the wind characteristics associated with seasonality.

Based on the above arguments, a shallow-water whiting phenomenon is proposed to explain the precipitation of aragonite needles in the Middle Miocene Bahamian carbonate ramp. This, in turn, suggests that despite the difference in bank morphology, the modern GBB platform and the Middle Miocene ramp display similar environmental properties both enabling whiting-related aragonite precipitation. As for the present-day settings, it is difficult to determine the origin of the whiting phenomenon in Middle Miocene. However, hydrodynamic processes and the geochemical state on the carbonate ramp could have led to whiting production by bottom sediments re-suspension and/or a biotically induced precipitation.

Conclusions

The granulometric separation of Middle Miocene sediments from Sites 1006 and 1007, located on the western margin of the GBB, allows for a detailed examination of the <12 μm fractions of carbonate muds. This approach sheds light on the location and precipitation mode of needle-shaped aragonite. The isotopic signature of separated fractions from unlithified and lithified sediments at Sites 1006 and 1007 is apparently pristine and reflects a primary signal combining seawater temperature and salinity effects.

Isotope ratios and Sr concentrations of aragonite-rich fractions and the morphology of aragonite crystals indicate that these needles have two possible origins: (1) a predominant whiting-related precipitation corresponding to a biotically induced precipitation on the bank and/or a bottom sediments re-suspension and (2) a minor proportion of fragmented codiacean algae. Both sources show that aragonite needles were formed in the shallow-water environment. This implies that the Miocene ramp morphology of GBB allows for whiting-related aragonite precipitation as observed for the Plio-Pleistocene rimmed, flat-topped platform.

Preservation of aragonite needles at distal sites suggests an allochtonous origin and suspension transport from the bank top towards the basin. The absence of preserved aragonite needles at slope Sites 1003 and 1005 suggests dissolution–recrystallization processes due to fluid circulation in the subsurface.

This study highlights the potential of granulometric separation and fraction-specific microscopical and geochemical analysis. In particular, the discrimination of primary versus diagenetic signals is instrumental to the understanding of processes active in modern and ancient carbonate settings.

Acknowledgments We would like to thank N. Labourdette, M. Person and J. Benmamar (Laboratoire Biominéralisations et Environnements sédimentaires, UPMC) for their technical assistance. A-F. Maurer is acknowledged for statistical analyses of the datasets and C. Beltran for helpful discussions. UPMC and VU University Amsterdam (to J. R.) are thanked for financial support. We are grateful to A. Immenhauser for his helpful suggestions during the preparation of the manuscript. Comments on an earlier version of the manuscript by P. Swart, T. Frank, E. Shinn and L. Reuning are acknowledged. An anonymous reviewer and associate editor Dan Bosence are thanked for their reviews of the revised version of the manuscript. C. Dullo is thanked for the editorial handling of the manuscript.

References

Anselmetti FS, Eberli GP, Ding ZO (2000) From the Great Bahama Bank into the Straits of Florida: a margin architecture controlled by sea-level fluctuations and ocean currents. GSA Bull 112: 829–844

Austin JA, Ewing JI, Ladd JW, Mullins HT, Sheridan RE (1988) Seismic stratigraphic implications of ODP Leg 101 Site surveys. In: Proceedings of ODP, science results, vol 101, pp 391–424

Bathurst RGC (1975) Carbonate sediments and their diagenesis. Developments in sedimentology, 12. Elsevier, Amsterdam, p 658

Beach DK, Ginsburg RN (1980) Facies succession of Pliocene-Pleistocene carbonates, northwestern Great Bahama Bank. AAPG Bull 64:1634–1642

Beltran C, de Rafélis M, Person A, Stalport F, Renard M (2009) Multiproxy approach for determination of nature and origin of carbonate micro-particles so-called "micarb" in pelagic sediments. Sediment Geol 213(1–2):64–76

Bernet KH, Eberli GP, Gilli A (2000) Turbidite frequency and composition in the distal part of the Bahamas Transect. In: Swart PK, Eberli GP, Malone MJ, Sarg JF (eds) Proceedings of ODP, science results, vol 166, pp 45–60

Betzler C, Reijmer JJG, Bernet K, Eberli GP, Anselmetti FS (1999) Sedimentary patterns and geometries of the Bahamian outer carbonate ramp (Miocene-Lower Pliocene, Great Bahama Bank). Sedimentology 46:1127–1143

Betzler C, Pfeiffer M, Saxena S (2000) Carbonate shedding and sedimentary cyclicities of a distally steepened carbonate ramp (Miocene, Great Bahama Bank). Int J Earth Sci 89:140–153

Broecker WS, Takahashi T (1966) Calcium carbonate precipitation on the Bahama Banks. J Geophys Res 71:1575–1602

Broecker WS, Sanyal A, Takahashi T (2000) The origin of Bahamian whitings revisited. Geophys Res Lett 27:3759–3760

Burchette TP, Wright VP (1992) Carbonate ramp depositional systems. Sediment Geol 79:3–57

Caspard E, Rudkiewicz JL, Eberli GP, Brosse E, Renard M (2004) Massive dolomitization of a Messinian reef in the Great Bahama Bank: a numerical modelling evaluation of Kohout geothermal convection. Geofluids 4:40–60

Cloud PEJ (1962a) Environment of calcium carbonate deposition west of Andros Island, Bahamas. US Geol Surv Prof Pap 350:1–138

Cloud PEJ (1962b) Behaviour of calcium carbonate in seawater. Geochim Cosmochim Acta 39:867–884

Cook HE, Egbert RM (1983) Diagenesis of deep-sea carbonates. In: Larsen G, Chilingar GV (eds) Diagenesis in sediments and sedimentary rocks 2. Development in sedimentology. Elsevier, Amsterdam, pp 213–288

De Groot K (1965) Inorganic precipitation of calcium carbonate from seawater. Nature 207:404–405

Demicco RV, Hardie LA (2002) The "carbonate factory" revisited: a reexamination of sediment production functions used to model deposition on carbonate platforms. J Sediment Res 72:849–857

Dierssen HM, Zimmerman RC, Burdige DJ (2009) Optics and remote sensing of Bahamian carbonate sediment whitings and potential relationship to wind-driven Langmuir circulation. Biogeosciences 6:487–500

Dix GR, James NP, Kyser TK, Bone Y, Collins LB (2005) Genesis and dispersal of carbonate mud relative to late quaternary sea-level change along a distally-steepened carbonate ramp (northwestern shelf, western Australia). J Sediment Res 75:665–678

Droxler AW, Schlager W (1985) Glacial versus interglacial sedimentation rates and turbidite frequency in the Bahamas. Geology 13:799–802

Duan Z, Sun R (2003) An improved model calculating CO_2 solubility in pure water and aqueous NaCl solutions from 273 to 533 K and from 0 to 2000 bar. Chem Geol 193:257–271

Eberli GP (2000) The record of Neogene sea-level changes in the prograding carbonates along the Bahamas Transect—Leg 166 synthesis. In: Proceedings of ODP, science results, vol 166, pp 167–177

Eberli GP, Ginsburg RN (1989) Cenozoic progradation of northwestern Great Bahama Bank, a record of lateral platform growth and sea-level fluctuations. In: Crevello PD, Wilson JL, Sarg JF, Read JF (eds) Controls on carbonate platform and basin development. SEPM, pp 339–351

Eberli GP, Swart PK, Malone MJ et al (1997) In: Proceedings of ODP, initial report 166

Eberli GP, Anselmetti FS, Kroon D, Sato T, Wright JD (2002) The chronostratigraphic significance of seismic reflections along the Bahamas Transect. Mar Geol 185:1–17

Effler SW, Johnson DL (1987) Calcium carbonate precipitation and turbidity measurements in Otisco Lake, NY. Water Resour Bull 23:73–79

Emrich K, Ehhalt EH, Vogel JC (1970) Carbon isotopic fractionation during the precipitation of calcium carbonate. Earth Planet Sci Lett 8:363–371

Epstein S, Buchsbaum R, Lowenstam HA, Urey HC (1953) Revised carbonate-water isotopic temperature scale. Geol Soc Am Bull 64:1315–1326

Erba E (1992) Calcareous nannofossils distribution in pelagic rhythmic sediments (Aptian-Albian Piobbico Core, Central Italy). Riv Ital Paleontol Stratigr 97:455–484

Frank TD, Bernet K (2000) Isotopic signature of burial diagenesis and primary lithological contrats in periplatform carbonates (Miocene, Great Bahama Bank). Sedimentology 47:1119–1134

Ginsburg RN (1956) Environmental relationships of grain size and constituent particles in some South Florida carbonate sediments. AAPG Bull 40:2384–2427

Gischler E, Zingeler D (2002) The origin of carbonate mud in isolated carbonate platforms of Belize, Central America. IJES 91:1054–1070

Gischler E, Swart PK, Lomando AJ (2009) Stable isotopes of carbon and oxygen in modern sediments of carbonate platforms, barrier reefs, atolls and ramps: patterns and implications. In: Swart PK, Eberli GP, McKenzie JA (eds) Perspectives in sedimentary geology: a tribute to the career of Robert Nathan Ginsburg. Blackwell, Oxford, IAS Spec Publ 41, pp 61–74

Gonzalez LA, Lohmann KC (1985) Carbon and oxygen isotopic composition of Holocene reefal carbonates. Geology 13:811–814

Heath KC, Mullins HT (1984) Open ocean off-bank transport of fine-grained carbonate sediment in the Northern Bahamas. In: Stow DAB, Piper DJW (eds) Fine-grained sediments: deep water processes and facies. Blackwell, London, pp 199–208

Immenhauser A, Kenter JAM, Ganssen G, Bahamonde JR, van Vliet A, Saher MH (2002) Origin and significance of isotope shifts in Pennsylvanian carbonates (Asturias, NW Spain). J Sediment Res 72:82–94

Immenhauser A, Holmden C, Patterson WP (2008) Interpreting the carbon-isotope record of ancient shallow epeiric seas: lessons from the Recent. In: Pratt BR, Holmden C (eds) Dynamics of Epeiric Seas. Geol Assoc Canada Spec Publ, pp 135–174

Isern AR, Anselmetti FS (2001) The influence of carbonate platform morphology and sea-level on fifth-order petrophysical cyclicity in slope and basin sediments adjacent to the Great Bahama Bank. Mar Geol 177:381–394

Kinsman DJJ (1969) Interpretation of Sr^{2+} concentrations in carbonate minerals and rocks. J Sediment Petrol 39:486–508

Kramer PA, Swart PK, DeCarlo EH, Schovsbo NH (2000) Overview of interstitial fluid and sediment geochemistry, sites 1003-1007 (Bahamas transect). In: Proceedings pf ODP, science results, vol 166, pp 179–195

Lalli CM, Gilmer RW (1989) Pelagic snails. The biology of holoplanktonic gastropod mollusks. Stanford University Press, Stanford, p 259

Lee D, Carpenter SJ (2001) Isotopic disequilibrium in marine calcareous algae. Chem Geol 172:307–329

Loreau JP (1982) Sédiments aragonitiques et leur genèse. Mémoires du Muséum d'Histoire Naturelle 47, Série C, pp 312

Lowenstam HA, Epstein S (1957) On the origin of sedimentary aragonite needles of the Great Bahama Bank. J Geol 65:364–375

Macintyre IG, Reid RP (1992) Comment on the origin of aragonite needle mud: a picture is worth a thousand words. J Sediment Petrol 62:1095–1097

Macintyre IG, Reid RP (1995) Crystal alteration in a living calcareous alga (*Halimeda*): implications for studies in skeletal diagenesis. J Sediment Res A65:143–153

Mathews RK (1966) Genesis of recent lime mud in southern British Honduras. J Sediment Petrol 36:428–454

Mattioli E, Pittet B (2002) Contribution of calcareous nannoplankton to carbonate deposition: a new approach applied to the Lower Jurassic of central Italy. Mar Micropaleontol 45:175–190

Mazzulo SJ, Bischoff WD, Teal CS (1995) Holocene shallow-subtidal dolomitization by near-normal seawater, northern Belize. Geology 23:341–344

McCave IN (1972) Transport and escape of fine-grained sediment from shelf areas. In: Swift DJP, Duane DB, Pilkey OH (eds) Shelf sediment transport. Dowden, Hutchinson and Ross Inc, Stroudsberg, pp 225–248

Milliman JD (1974) Marine carbonates. Springer, Berlin, p 375

Milliman JD, Freile D, Steinen RP, Wilber RJ (1993) Great Bahama Bank aragonitic muds: mostly inorganically precipitated, mostly exported. J Sediment Petrol 63:589–595

Minoletti F (2002) Mise au point d'un protocole de séparation des assemblages de nannofossiles calcaires. Apport à la micropaléontologie et à la géochimie des producteurs carbonatés pélagiques. Application à la crise Crétacé-Tertiaire. PhD thesis, University of Pierre et Marie Curie, Paris, pp 248

Minoletti F, deRafélis M, Renard M, Gardin S, Young J (2005) Changes in the pelagic fine fraction carbonate sedimentation during the Cretaceous-Paleocene transition: contribution of the separation technique to the study of Bidart section. Palaeogeogr Palaeoclimatol Palaeoecol 216:119–137

Morse JW, Mackenzie FT (1990) Geochemistry of sedimentary carbonates. Developments in sedimentology 48. Elsevier, Amsterdam, p 707

Morse JW, Millero FJ, Thurmond V, Brown E, Ostlund HG (1984) The carbonate chemistry of Grand Bahama Bank waters: after 18 years another look. J Geophys Res 89:3604–3614

Neev D, Emery KO (1967) The Dead Sea: depositional processes and environment of evaporites. Jerusalem Geol Surv Bull 41:1–147

Neumann AC, Land LS (1975) Lime mud deposition and calcareous algae in the Bight of Abaco, Bahamas: a budget. J Sediment Petrol 45:763–786

Petschik R (1991) MacDiff Manual 4.0.7. Frankfurt

Preto N, Spötl C, Guaiumi C (2009) Evaluation of bulk carbonate δ13C data from Triassic hemipelagites and the initial composition of carbonate mud. Sedimentology 56(5):1329–1345

Purdy EG (1963a) Recent calcium carbonate facies of the Great Bahama Bank. 1. Petrography and reaction groups. J Geol 71:334–355

Purdy EG (1963b) Recent calcium carbonate facies of the Great Bahama Bank. 2. Sedimentary facies. J Geol 71:472–497

Purdy EG, Gischler E (2003) The Belize margin revisited: 1. Holocene marine facies. Int J Earth Sci 92:532–551

Reijmer JJG, Schlager W, Bosscher H, Beets CJ, McNeill DF (1992) Pliocene/Pleistocene platform facies transition recorded in calciturbidites (Exuma Sound Bahamas). Sediment Geol 78:171–179

Reijmer JJG, Betzler C, Kroon D, Tiedemann R, Eberli GP (2002) Bahamian carbonate platform development in response to sea-level changes and the closure of the Isthmus of Panama. Int J Earth Sci 91:482–489

Reijmer JJG, Swart PK, Bauch T, Otto R, Reuning L, Roth S, Zechel S (2009) A reevaluation of facies on Great Bahama Bank I: New facies maps of Western Great Bahama Bank. In: Swart PK, Eberli GP, McKenzie JA (eds) Perspectives in sedimentary geology: a tribute to the career of Robert Nathan Ginsburg. Blackwell, Oxford, IAS Spec Publ 41, pp 29–46

Rendle-Bühring RH, Reijmer JJG (2005) Controls on grain-size patterns in periplatform carbonates: marginal setting versus glacio-eustacy. Sediment Geol 175:99–113

Reuning L, Reijmer JJG, Betzler C (2002) Sedimentation cycles and their diagenesis on the slope of a Miocene carbonate ramp (Bahamas, ODP Leg 166). Mar Geol 185:121–142

Robbins LL, Blackwelder PL (1992) Biochemical and ultrastructural evidence for the origin of whitings: a biologically induced calcium carbonate precipitation mechanism. Geology 20:464–468

Robbins LL, Yates KK, Shinn EA, Blackwelder PL (1996) Whitings on the Great Bahama Bank: a microscopic solution to a macroscopic mystery. Bahamas J Sci 4:1–7

Robbins LL, Tao Y, Evans CA (1997) Temporal and spatial distribution of whitings on Great Bahama Bank and a new lime mud budget. Geology 25:947–950

Roth S, Reijmer JJG (2005) Holocene millenial to centennial carbonate cyclicity recorded in slope sediments of the Great Bahama Bank and its climatic implications. Sedimentology 52:161–181

Sandberg PA (1975) Bryozoan diagenesis: bearing on the nature of the original skeleton of rugose corals. J Paleontol 49:587–606

Schlager W, Chermak A (1979) Sediment facies of platform-basin transition, tongue of the Ocean, Bahamas. SEPM Spec Publ 27:193–208

Schlager W, Reijmer JJG, Droxler AW (1994) Highstand shedding of carbonate platforms. J Sediment Res B64:270–281

Shackleton NJ, Kennett JP (1975) Paleotemperature history of the Cenozoic and the initiation of Antarctic glaciation; oxygen and carbon isotope analysis in DSDP sites 277, 279 and 281. Init Rep DSDP 29:743–755

Shinn EA, Steinen RP, Lidz BH, Swart PK (1989) Whitings, a sedimentologic dilemma. J Sediment Petrol 59:147–161

Shinn EA, Holmes CW, Marot M (2000) Short-lived isotopes for investigation of microbially precipitated calcium carbonate: A new approach to the "whiting problem". Geol Soc Am Abstr Prog 32(7):A279

Shinn EA, Marot M, Holmes CW (2004) Solving the whiting problem with short-lived isotopes: Still no Fish. AAPG Bull 88(13)

Sondi I, Juračič M (2010) Whiting events and the formation of aragonite in Mediterranean Karstic Marine Lakes: new evidence on its biologically induced inorganic origin. Sedimentology 57:85–95

Stanley SM, Hardie LA (1998) Secular oscillations in the carbonate mineralogy of reef-building and sediment-producing organisms driven by tectonically forced shifts in seawater chemistry. Palaeogeogr Palaeoclimatol Palaeoecol 144:3–19

Stockman KW, Ginsburg RN, Shinn EA (1967) The production of lime mud by algae in south Florida. J Sediment Petrol 37:633–648

Strong AE, Eadie BJ (1978) Satellite observations of calcium carbonate precipitations in the Great Lakes. Limnol Oceanogr 23:877–887

Swart PK (2000) The oxygen isotopic composition of interstitial waters: evidence for fluid flow and recrystallization in the margin of the Great Bahama Bank. In: Swart PK, Eberli GP, Malone MJ, Sarg JF (eds) Proceedings of ODP, science results, vol 166, pp 91–98

Swart PK (2002) Recrystallisation and carbon isotopic composition of pore waters associated with the diagenesis of periplatform sediments. AAPG Abstr 11:A171

Swart PK, Eberli G (2005) The nature of the $\delta^{13}C$ of periplatform sediments: implications for stratigraphy and the global carbon cycle. Sediment Geol 175:115–129

Swart PK, Reijmer JJG, Otto R (2009) A reevaluation of facies on Great Bahama Bank II: Variations in the $\delta^{13}C$, $\delta^{18}O$, and mineralogy of surface sediments. In: Swart PK, Eberli GP, McKenzie JA (eds) Perspectives in sedimentary geology: a tribute to the career of Robert Nathan Ginsburg. Blackwell, Oxford, IAS Spec Publ 41, pp 47–60

Tao Y (1994) Whitings on the Great Bahama Bank: distribution in space and time using space shuttle photographs. Master Thesis, University of South Florida, Tampa, pp 77

Tarutani T, Clayton RN, Mayeda TK (1969) Effect of polymorphism and magnesium substitution on oxygen isotope fractionation between calcium carbonate and water. Geochim Cosmochim Acta 33:987–996

Thompson JB (2000) Microbial whitings. In: Riding RE, Awramik SM (eds) Microbial sediments. Springer, Berlin, pp 250–260

Thompson JB, Ferris FG (1990) Cyanobacterial precipitation of gypsum, calcite, magnesite from natural alkaline lake water. Geology 18:995–998

Thompson JB, Schultze-Lam S, Beveridge TJ, DesMarais DJ (1997) Whiting events: biogenic origin due to photosynthetic activity of cyanobacterial picoplankton. Limnol Oceanogr 42:133–141

Thorpe S (2004) Langmuir circulation. Annu Rev Fluid Mech 36:55–79

Turner JV (1982) Kinetic fractionation of carbon-13 during calcium carbonate precipitation. Geochim Cosmochim Acta 46:1183–1191

Turpin M (2006) Caractérisation minéralogique et géochimique de la sédimentation carbonatée en domaine de péri plate-forme: Mise en évidence de l'influence des processus d'exportation à partir des exemples des Bahamas au Miocène et de la Maiella (Italie) au Crétacé. PhD thesis, University of Pierre et Marie Curie, Paris, pp 275

Turpin M, Emmanuel L, Renard M (2008) Nature and origin of carbonate particles along a transect on the western margin of Great Bahama Bank during the Middle Miocene: sedimentary processes and depositional model. Bull Soc Géol Fr 179(3):231–244

Tyrrell T, Merico A (2004) *Emiliania huxleyi*: bloom observations and the conditions that induce them. In: Thierstein HR, Young JR (eds) *Coccolithophores*: from molecular processes to global impact. Springer, Berlin, pp 75–97

van der Kooij B, Immenhauser A, Csoma A, Bahamonde J, Steuber T (2009) Spatial geochemistry of a Carboniferous platform-margin-to-basin transect: balancing environmental and diagenetic factors. Sediment Geol 219:136–150

van der Spoel S (1976) Pseudothecosomata, Gymnosomata and Heteropoda Gastropods. Bohn, Scheltema and Holkema, Utrecht, p 484

Weber JN (1967) Factors affecting the carbon and oxygen isotopic composition of marine carbonate sediments—part I, Bermuda. Am J Sci 265:586–608

Weber JN, Woodhead PMJ (1969) Factors affecting the carbon and oxygen isotopic composition of marine carbonate sediments—II. Heron Island, Great Barrier Reef, Australia. Geochim Cosmochim Acta 33:19–38

Wells AJ, Illing LV (1964) Present-day precipitation of calcium carbonate in the Persian Gulf. In: van Straaten L (ed) Deltaic and shallow-water marine deposits. Elsevier Developments in Sedimentology Series, New York, pp 429–435

Wilber RJ, Milliman JD, Halley R (1990) Accumulation of bank-top sediment on the western slope of Great Bahama Bank: rapid progradation of a carbonate megabank. Geology 18:970–974

Wilson PA, Roberts HH (1992) Carbonate periplatform sedimentation by density flows: a mechanism for rapid off-bank and vertical transport of shallow-water fines. Geology 20:713–716

Wilson PA, Roberts HH (1995) Density cascading: off-shelf sediment transport, evidence and implications, Bahama Banks. J Sediment Res A65:45–56

Yates KK, Robbins LL (1995) Experimental evidence for a $CaCO_3$ precipitation mechanism for marine *Synechocystis*. Bull Inst Océanogr Monaco Numéro spécial 14(2):51–59

Yates KK, Robbins LL (1999) Radioisotopic tracer studies of inorganic carbon and Ca in microbially derived $CaCO_3$. Geochim Cosmochim Acta 63:129–136

Zachos JC, Dickens GR, Zeebe RE (2008) An early Cenozoic perspective on greenhouse warming and carbon-cycle dynamics. Nature 451:279–283